*Korean J. Chem. Eng.*, 34(1), 150-159 (2017)
DOI: 10.1007/s11814-016-0250-z

pISSN: 0256-1115
eISSN: 1975-7220

# Hydrodynamic characteristics of valve tray: Computational fluid dynamic simulation and experimental studies

**Taleb Zarei*, Masoud Farsiani**,†, and Jamshid Khorshidi***

*Department of Mechanical Engineering, University of Horrmozgan, Bandar Abbas, Iran
**Young Researchers and Elites Club, Sirjan Branch, Islamic Azad University, Sirjan, Iran
(*Received 13 February 2016 • accepted 31 August 2016*)

**Abstract**–In order to better understand the hydrodynamics of valve trays, air-water operation in an industrial scale tower with 1.2 m of diameter, consisting of two 14% valve trays, was studied. Experimental results of clear liquid height, froth height, average liquid holdup, dry pressure drop, total pressure drop, weeping and entrainment were investigated, and empirical correlations were presented. Then, a three-dimensional computational fluid dynamics (CFD) simulation in an Eulerian framework for valve tray with ANSYS CFX software was done. The drag coefficient, which was used in the CFD simulations, was calculated from the data obtained in the experiments. The simulation results were found to be in good agreement with experimental data at this industrial scale. The objective of the work was to study the extent to which experimental and CFD simulations must be used together as a prediction and design tool for industrial trays.

Keywords: Valve Tray, Computational Fluid Dynamics, Weeping, Entrainment, Clear Liquid Height

## INTRODUCTION

The separation operation is one of the most important issues that has been under the attention of industrialists and researchers. Efforts to increase efficiency and finding better ways, faster and cheaper separations are concentrated. Distillation tower trays are well known and useful in the separation and purification process. In this research, the valve tray, which is the most widely used tray type in the process industries, has been studied. Although many studies on distillation tower trays have been carried out, the number of published articles in the field of valve trays has been few. One of the first works in this field was done by Scheffe and Weiland [1], who investigated mass-transfer characteristics of valve trays. This study was done on an experimental scale. Mustafa and Békássy-Molnár [2] studied the hydrodynamic characteristics of Nutter valve trays and obtained new correlations for hydrodynamic parameters. In that work, the clear liquid height was determined in different operating regimes (foam with mixed and spray regimes) and new formulas were developed as functions of weir height and flow parameter. Wijn [3], studied the lower operating range of sieve and valve trays. Brahem et al. [4] did an experimental hydrodynamic study of valve trays and proposed correlations for clear liquid height, liquid mean holdup and emulsion height. The proposed correlations led to large discrepancies and thus more experimental works were required. In addition, the experimental works carried out often are in the form of experimental scale, and industrial scales are in the monopoly of reputable companies such as Fractionation Research Institute (FRI).

In spite of these few experimental articles, in recent years some reaserchers have introduced and utilized CFD modeling as powerful tool for tray design and for obtaining detailed information about the flow behavior. The initial CFD study on the distillation tray was carried out on the sieve tray because of simplicity of structure of this type of tray. Krishna et al. [5] did CFD simulations of sieve tray hydrodynamics. In this work the clear liquid height determined from these simulations was in reasonable agreement with experimental measurements carried out for the air-water in a rectangular tray. Van Baten and Krishna [6] carried out a modelling sieve tray hydraulics using computational fluid dynamics. The CFD simulations reflected chaotic tray hydrodynamics and revealed several liquid circulation patterns. The clear liquid height determined from these simulations was in good agreement with the Bennett correlation. More of these works have been done in the experimental scale, so more research would be needed on an industrial scale. Gesit et al. [7] did CFD modeling of flow patterns and hydraulics of commericial-scale sieve trays. The simulation results show that CFD can be used as an invaluable tool in tray design and analysis. Roshdi et al. [8] investigated a computational fluid dynamics simulation of multiphase flow in packed sieve tray of a distillation column. The simulation results showed that 3.08 cm of packing thickness could increase the clear liquid height up to 17 percent and froth height up to 10 percent, as well as promoting froth density by 6 percent with the only drawback of increasing wet pressure drop up to 16 percent in froth regime. Zarei et al. [9] performed a CFD study of weeping rate in the rectangular sieve trays. In this research an Eulerian-Eulerian computational fluid dynamics (CFD) method was executed. The obtained CFD results are in a good agreement with the experimental data and Zuiderweg [10] empirical correlation data in terms of weeping rate and pressure drop, respectively.

In the following, the CFD simulation of valve tray was also considered by some researchers. Most of the CFD model was based on

†To whom correspondence should be addressed.
E-mail: masoudfarsiani@yahoo.com

the previous models for the sieve tray. In the lack of reported experimental data for the valve tray, the CFD simulation is a powerful tool for predicting the tray's behavior. Li et al. [11] investigated the CFD simulation of valve tray hydrodynamics. Based on the clear liquid height measured on a full open valve tray, a new correlation of liquid hold-up was developed, and the interphase momentum transfer term was calculated. Zarei et al. [12] discussed computational fluid dynamics simulation of MVG (Mini V-Grid) tray hydraulics. The simulation results for MVG tray are compared with that of the sieve tray. The sieve tray geometry and operating conditions are based on Solari and Bell's [13] sieve tray. CFD and experimental studies on the effect of valve weight on the performance of a valve tray column were investigated by Alizadehdakhel et al. [14]. To demonstrate the repeatability and consistency of the measurements, the results were analyzed using two-stage nested designs. Jiang et al. [15] studied modeling fixed triangular valve tray hydraulics using computational fluid dynamics. The gas and liquid phase, as two interpenetrating phases, were modeled on the Eulerian framework. Based on the clear liquid height obtained by experiments, a new correlation for liquid hold-up was adopted, and the interphase momentum transfer source was also calculated. Yufeng et al. [16] studied in CFD gas-liquid simulation of the oriented valve tray.

Although CFD has become a powerful research and design tool in valve trays, there are no reports on the simulation of the valve tray on an industrial scale with extensieve experimental data in normal, upper and lower operating limit.

In the present work with the aim of creating a better understanding of the valve trays' operation, we did a comprehensive study using experimental and CFD simulations in the industrial scale. The hydrodynamics tower includes two trays built and operations of the valve tray in hydrodynamic conditions are investigated. One of the important characterstics of the experimental pilot was reported as total pressure drop, dry pressure drop, weeping, entrainment, clear liquid height and froth height and average liquid holdup simultaneously. Furthermore, a three-dimensional gas-liquid two phase simulation in the Eulerian framework and on an industrial scale was done. ANSYS Workbench for geometry and meshing and ANSYS CFX15 for model building and solving equations were used in the simulations. The CFD results were compared with the experimental data.

## METHODS

### 1. Experimental

The hydrodynamics tower includes two valve trays made (Fig. 1) The atmospheric pressure and temperature of 25 °C as operating conditions were determined.

The valve trays characteristics were presented in Table 1.

1-1. The Air Pathway in the Column

Fig. 1 presents a schematic diagram of the tower. The different parts of the columns are numbered. The air from the blower under the tower (1) in a certain flow rate goes into the chimneys (2) and is distributed into the tower. Dry pressure drop indicates the amount of energy consumed gas phase for passes through the holes and in dealing with valves in the absence of a liquid phase. To measure the dry pressure drop in the experimental section, a graded manometer was used. The accuracy of this tool is ±0.05, water centimeter that approximately is 5 Pa. The total pressure drop is the result of the dry pressure drop and the pressure drop causes collision of two phases. To calculate this parameter, like the dry pressure drop, the graded manometer was used.

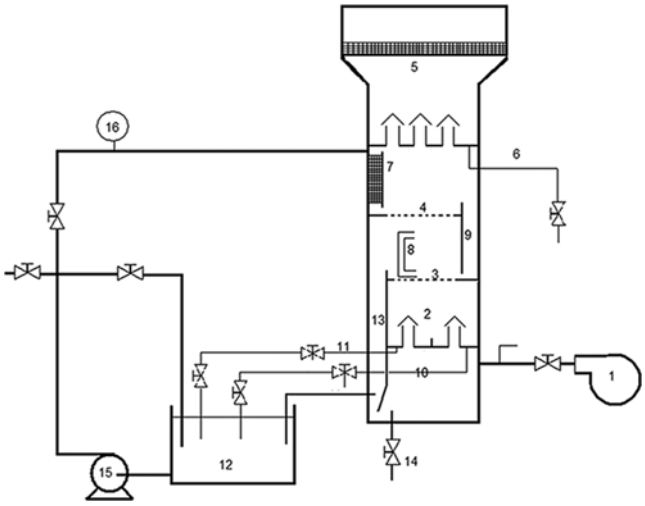


**Fig. 1. The schematic of the experimental pilot.**

**Table 1. The valve tray characterization**

| Characteristics | Number or size |
|---|---|
| Tower cross section diameter (m) | 1.22 |
| Tray diameter (m) | 1.2 |
| Weir height (mm) | 50 |
| Weir length (mm) | 760 |
| Number of valves | 118 |
| Tray thickness (mm) | 2 |
| Hole area percentage | 14% |
| Active area ($m^2$) | 1.00776 |
| Weight of valve (kg) | 0.024 |
| Height of reversal/riser (mm) | 12.5 |
| Downcomer clearance (mm) | 38 |
| Tray spacing (mm) | 610 |

In the following and after contacting between two phases on the bottom tray (3), the air goes out of this space and then continues its vertical movement and enters into the upper tray (4). After re-interference of phases in the upper tray, the gas continues to vertically move to top direction. To calculate the entrainment rate, the upper tray was considered. Then, a chimney tray on the above of the tray was installed and on top of that, the demister pad (dehumidifiers) were placed (5). When entrained water droplet in a gas stream contacted with the demister pad, liquid droplets were removed and fell on the tray. Then, they were collected and moved out via a valve (6) and measured. Finally, the gas phase operation was completed and went out of the tower.

1-2. Liquid Pathway in the Column

The water enters the tower after passing through an unstructural packing (7) in the downcomer of the upper tray. The height

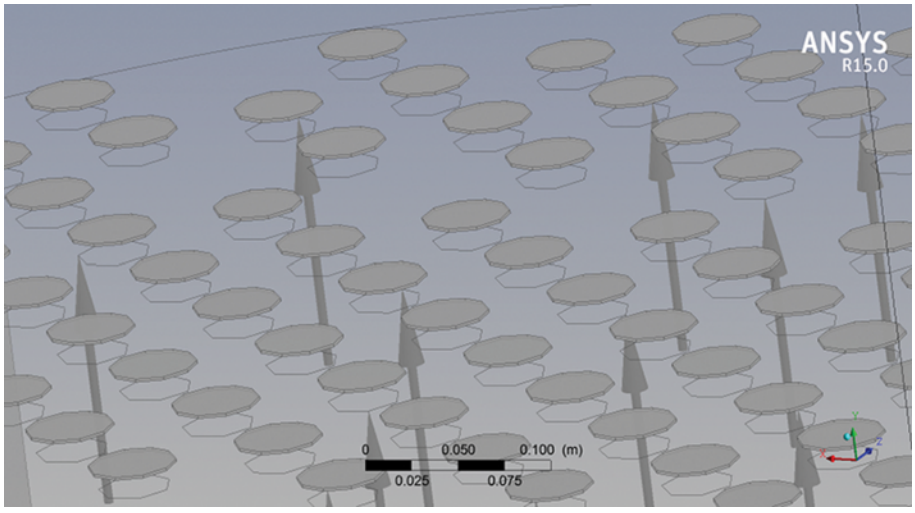


**Fig. 2. The geometry of the valve tray deck.**

of the liquid on the tray in the absence of the incoming gas is called clear liquid height. To calculate the amount of this parameter in the experimental part, a U-shaped manometer was used. The manometer on the wall of the tower was installed. One side of the manometer was connected to the bottom of the tray and the other side to above the froth region of the tray (8). In each operating condition, the height of the liquid inside the tube manometer was the clear liquid height. Furthermore, for measuring the froth height, visual method was used.

Froth height that formed a layer of spume on top of the tray could be measured with a ruler which was located vertically on the tray deck. For this purpose, a specified operating condition was fixed for 10 to 15 minutes operations to achieve steady state condition. After froth height measurements, operating conditions were changed.

The average liquid holdup is the clear liquid height to froth height ratio [17]. Therefore, this parameter was calculated indirectly from clear liquid and froth height measurments.

Prediction of the onset and the rate of weeping is one of the important issues in tray hydrodynamics. Heavy weeping can affect the tray efficiency, especially when the weeping percent gets more than 20% [18].

To calculate this parameter in the experimental section, the lower tray is intended. To do so, a chimney tray was mounted under the tray. This tray collects the weeping liquid of the desired valve tray. Then the liquid flows via valves installed below the chimney tray (10 and 11) is moved to a tank (12) and measured to obtain the amount of weeping. Apart from the amount of liquid calculated in the section of weeping and entrainment, a significant portion of the liquid through the downcomer (13) was transmitted down to the bottom of the tower and by a valve (14), was out and came back to the return cycle.

## 2. CFD Modeling

The model takes the flow of gas and liquid in the Eulerian-Eulerian framework in which each phase is handled as an interpenetrating continuum having separate transport equations. With the model focusing on the froth region of the tray, the gas phase was taken as the dispersed phase, while the liquid phase formed the continuous phase [12]. An air-water simulation in the Eulerian framework in three-dimensional and transient mode was carried out. As it can be seen in Fig. 2, the valves in pill form on the top of holes are considered. Valves floats as valve hole gas velocity is changing. When the velocity of gas passing through the valve hole is larger than a certain value, the critical valve hole velocity, the valve is fully open. It means that the valve lifts with the maximum extent and it does not float. The CFD model was developed in this full open valve tray condition.

A whole tray was modeled, One of the problems in tray geometry modeling is to specify the geometry of valves for CFD simulations. In the present modeling, the valves were integrated with other computational space. Just the top face of valves was considered as a wall. Except the top faces of valves, other faces were used as interior faces of solution domain and all phases could pass through.

### 2-1. Model Equations

A multiphase flow system contains a mixture of phases that may have different flow fields, such as different velocity, pressure, and temperature [19]. In this simulation, Eulerian-Eulerian method for solving the multiphase flow was used. The Eulerain-Eulerain model is a famous multiphase model. In the multi-fluid modeling approach, each phase possesses its own flow field, so each phase has its own temperature, velocity etc., field. Each point in the mixture is occupied simultaneously by each phase. Therefore, the phases are considered as interpenetrating continua. Each phase is governed by its own conservation and constitutive equations; these are then coupled through interphase transfer [20]. Computational fluid dynamics uses continuity and momentum equations for solving issues. In this method, liquid phase as continuous phase and gas phase as dispersed phase are considered, and the relation between the two phases by drag force is defined. The equations are given below:

$$\alpha_G + \alpha_L = 1 \tag{1}$$

In Eq. (1), $\alpha_L$ and $\alpha_G$ are average liquid hold up and average gas

holdup that are linked by this relation.

2-1-1. Continuity Equation

Gas phase:

$$\frac{\partial(\alpha_G\rho_G)}{\partial t}+\nabla\cdot(\alpha_G\rho_G V_G)=0 \quad (2)$$

Liquid phase:

$$\frac{\partial(\alpha_L\rho_L)}{\partial t}+\nabla\cdot(\alpha_L\rho_L V_L)=0 \quad (3)$$

2-1-2. Momentum Equation

Gas phase:

$$\frac{\partial}{\partial t}(\alpha_G\rho_G V_G)+\nabla\cdot(\alpha_G(\rho_G V_G V_G)) = -\alpha_G\nabla P_G - M_{GL}+\nabla\cdot(\alpha_G\mu_{eff,G}(\nabla V_G+(\nabla V_G)^T)) \quad (4)$$

Liquid phase:

$$\frac{\partial}{\partial t}(\alpha_L\rho_L V_L)+\nabla\cdot(\alpha_L(\rho_L V_L V_L)) = -\alpha_L\nabla P_L + M_{GL}+\nabla\cdot(\alpha_L\mu_{eff,L}(\nabla V_L+(\nabla V_L)^T)) \quad (5)$$

2-1-3. Drag Force

The gas phase is the dispersed phase, the equation is written as follows:

$$M_{GL}=\frac{3}{4}\frac{C_D}{d_G}\alpha_G\rho_L|V_G-V_L|(V_G-V_L) \quad (6)$$

In Eq. (6), $C_D$ is drag coefficient or the momentum transfer coefficient between the phases. In the conditions of large bubbles, van Baten and Krishna [5] proposed Eq. (7) for the drag coffiecient:

$$C_D=\frac{3}{4}((\rho_L-\rho_G)/\rho_L)gd_G(1/V_{slip}^2) \quad (7)$$

$V_{slip}$ is slip velocity between gas and liquid which is defined as follows:

$$V_{slip}=|U_G-U_L| \quad (8)$$

For the average gas holdup ($\alpha_G$) in Eq. (6), the previous researchers used the Bennet et al. [21] empirical correlation. But, in this article, gas holdup data that were extracted in the present experiment was used. Certainly, correlation data (which was derived for sieve tray) has some deviation from the actual data. In this study experimental and CFD model cover each other.

2-2. Turbulence Model

One of the main issues in the simulations is the choice of the turbulence model. In this simulation, the k-$\varepsilon$ standard model was used. Universality, credibility and high accuracy of the model were the main reasons for this choice. This model is an acceptable model that was used by other researchers in previous simulations ed [22].

2-3. Geometry and Meshing

In this research, a three-dimensional geometry was designed that was based on an industrial scale. To increase accuracy, the whole tray geometry associated with exit downcomer was considered. In the pilot experiment, two test trays were used. The air-water flow regime gets closer to reality on the tray. For example, the bottom test tray shows that weeping is more accurate than upper test tray, because the liquid distribution from its downcommer is closer to reality. But, in the CFD simulation, selecting a good computational space depends on clear boundary condition and computational time (tray has an industrial scale). In this model, the bottom test tray was selected without any symmetry assumption and CFD data was compared with the experimental data of the bottom test tray. In most of the previous tray simulations, only half of the tray was modeled so as to save computational time and memory [7,12].

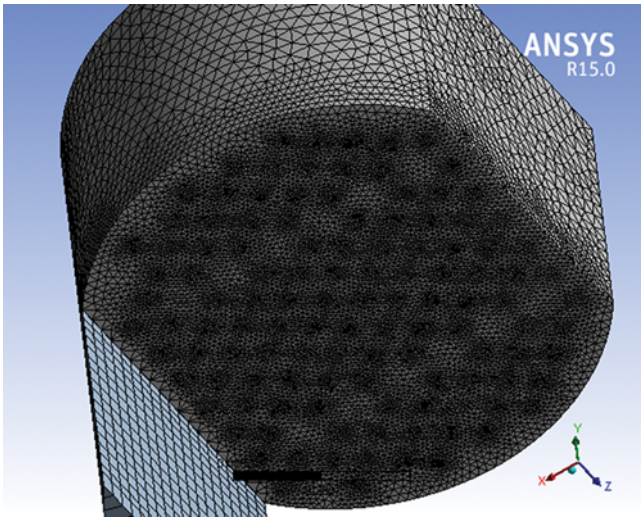


**Fig. 3. Meshing of the computational domain.**

Selection of the type and number of grids in simulation is very important. Done properly, the work, in convergence, accuracy of the results and model final quality, is very impressive.

Fig. 3 shows the tray geometry and its hybrid mesh. The hybrid mesh consists of the tetrahedral, wedge and prism mesh. This unstructural mesh was chosen because of the complex geometry of the valve tray.

Independence from the mesh

The high number of the grids increases cost and depreciation and computational time, so it is very important to determine the threshold of independence from the mesh. Therefore, for the mesh independency, four different mesh sizes were simulated. The clear liquid height parameter was used for comparison. Table 2 shows the clear liquid height for the four different mesh sizes in a constant operating condition. The results show that the clear liquid height was not changed considerably in the simulations with the number of nods more than 172000. Then, 172000 nods was used in the simulations.

2-4. Boundary Conditions

One of the important points that affect the convergence and

**Table 2. The clear liquid height in the four various nods**

| Number of nods | Clear liquid height (m) |
|---|---|
| 123000 | 0.039363154 |
| 172000 | 0.033556946 |
| 202000 | 0.033497048 |
| 291000 | 0.033279213 |

quality of the results is a suitable boundary condition's selection. Inappropriate choice of the boundary conditions may cause divergence in the simulations. Therefore, the appropriate and reasonable initial and boundary conditions for phases are necessary and important [23].

2-5. Gas Inlet

The inlet gas velocity:

$$V_{Airin}=V_S(A_{area}/A_{holes}) \quad (9)$$

$V_S$ is superficial gas velocity and $A_{holes}$ is the holes surface area and $A_{area}$ is the active area of the tray.

$$A_{holes}=118A_{hole} \quad (10)$$

2-6. Liquid Inlet

A parabolic profile was considered to the inlet liquid velocity [12]. There is a suitable agreement between the inlet and the outlet liquid in order to prevent liquid accumulation and an imbalance in the system.

Eq. (11) is the parabolic liquid inlet velocity profile:

$$U_{L,\,in}=1.5\frac{Q_L}{h_{ap}\times L_{Weir}}\left[1-\left(\frac{2z}{L_{Weir}}\right)^2\right] \quad (11)$$

2-7. Wall

To determine the general status of phases and increase the accuracy of solution near the walls, wall boundary conditions in the best mode must be defined. The most common of wall boundary condition is no-slip for liquid phase and free slip boundary condition for gas phase. So, the velocity of the liquid phase movement and also gradient of other variables related to this phase near the walls are considered to be zero.

2-8. Outlets

The liquid and gas outlet streams are shown in Fig. 4. To adjust the outlet boundary conditions, pressure parameters were used. The relative pressure was considered zero for the outlet boundary conditions. Due to the importance of correct solving of equations at outlet boundaries, determining these boundary conditions is of particular sensitivity.

2-9. Initial Conditions

The initial conditions must be determined and a certain and suitable initial amount for all indeterminate amounts of the issue assigned.

Resonable initial conditions must be specified at any specific internal boundaries of the flow geometry. Approporate initial guesses of the flow parameters are important to computational time and avoiding divergence [24]. Water and air at room temperature and atmospheric pressure were the fluids used in the simulation.

Such issues that are time-related are better as the initial values; the actual amounts of the start of experimental operation must be considered.

In a complex simulation, more accurate determination of these values is very important. The simulation has been run transient, and this selection is for getting better results and more principled. The results of the transient run of this simulation in the first showed the fluctuation mode; then these fluctuations as shown in Fig. 5, after 6 seconds to quasi-steady state is reached. That's why as the duration of this project 10 seconds was considered until the fluctuations were covered. Time step in this work of 0.001 seconds was considered. Also, the clear liquid height for initial condition for the simulation is 0.05 meters. This value is defined by considering the average of clear liquid heights obtained from experimental work and average of this heights results of the unsteady state.

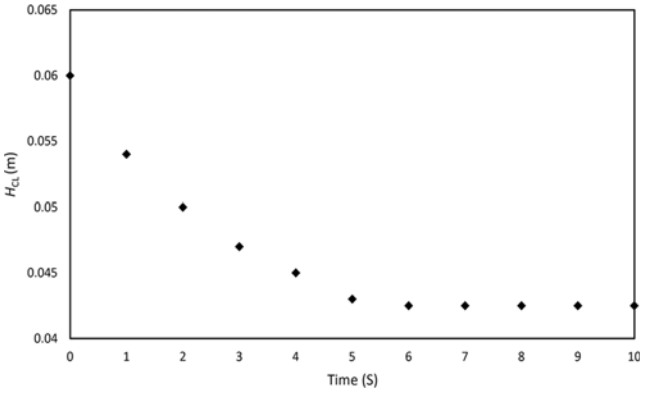


**Fig. 5. Transient simulation convergence by plot of clear liquid height VS. time.**

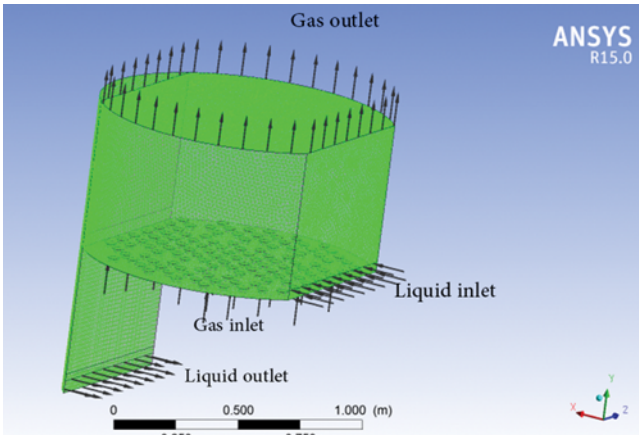


**Fig. 4. Gas and liquid boundary conditions.**

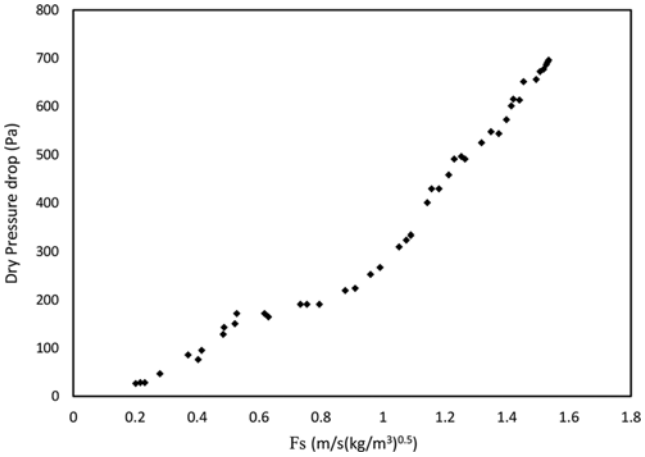


**Fig. 6. The dry pressure drop vs. $F_s$ for the valve tray.**

## RESULTS AND DISCUSSION

### 1. Experimental

1-1. Dry Pressure Drop

Fig. 6 shows the dry pressure drop vs. $F_S$. As shown, the dry pressure drop increases by increasing $F_s$. A steep slope was observed in the low gas velocity because a high pressure drop was consumed to open the valves. In the $F_S$=0.5 (m/s(kg/m$^3$)$^{0.5}$), by increasing the gas velocity the dry pressure drop approximately remains constant to the point where $F_s$=1 (m/s(kg/m$^3$)$^{0.5}$), because all valves are open and pressure drop is not used for valve opening. Where $F_S$ is greater than 1, again due to high increasing of gas velocity and increment the friction, pressure drop increases.

1-2. Total Pressure Drop

The total pressure drop is one of the most important parameters in the tray hydrodynamics. The results of the total pressure drop in Fig. 7 are shown. The total pressure drop is increasing with incrementing of the gas and liquid flow rate.

In addition, for these results and by charting compatible with data, the following empirical equation for total pressure drop based on the rate of gas and liquid was obtained:

$$\Delta P_T = 222.1F_s^2 + 1.77Q_L + 438.2 \quad (12)$$

$$R^2 = 0.92$$

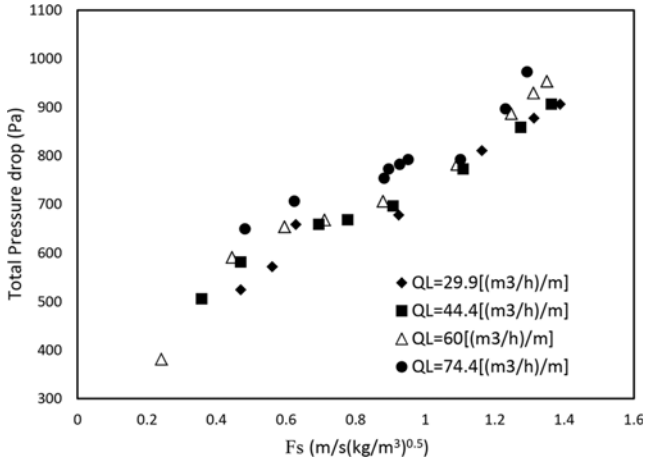


**Fig. 7. Total pressure drop of valve tray in the four liquid rates: $Q_L$= 29.9, 44.4, 60 and 74.4 (m$^3$/h)/m.**

1-3. Weeping

Weeping occurs when the hole gas velocity is insufficient to support the liquid. Therefore, weep rate varies with hole gas velocity [17]. Fig. 8 shows the weep rate versus F-factor and the onset of the weeping. The results show that the liquid rate did not have a significant effect on the amount of weeping. The cause of this phenomenon can be related to the role of valves.

According to Fig. 8, by increasing $F_s$, weeping decreases. Eq. (13) is based on the weeping experimental data.

$$\text{Weeping} = -0.007F_s^2 + (1.3\times10^{-5})Q_L + 0.006 \quad (13)$$

$$R^2 = 0.9$$

1-4. Entrainment

The prediction of the rate of entrainment is important for a check on the approach to flooding and also to predict the reduction in valve tray efficiency due to entainment. The trend of entrainment in Fig. 9 shows that with increasing F-factor, entrainment increases and this is via incrementing gas velocity.

In the following based on the entrainment experimental results, empirical Eq. (14) was found. The correlation can predict entrainment rate based on gas and liquid flow rates.

$$\text{Entrainment} = 0.003F_s^2 + (2\times10^{-5})Q_L + 0.0004 \quad (14)$$

$$R^2 = 0.95$$

### 2. CFD Simulation

2-1. Clear Liquid Height

If the operating conditions are not well determined or weeping and entrainment are more than the reasonable, clear liquid height may be less than expected, and this will have an adverse effect on the interfering phases, and finally the reduction in the tray efficiency. As can be seen in Fig. 10, due to gas and liquid contacting, an overlapping regime has been created onto the tray. Therefore, the clear liquid height is not measurable by the visual method so that another way must be used. In the simulation, the clear liquid height was obtained by multiplying the average water volume frac-

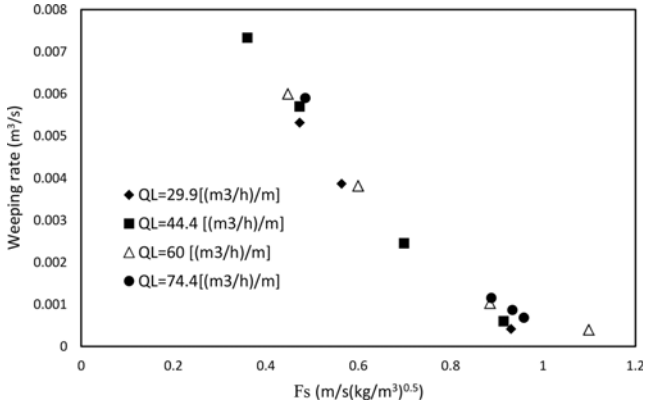


**Fig. 8. Weeping of valve tray in the various liquid flow rate: $Q_L$=29.9, 44.4, 60 and 74.4 (m$^3$/h)/m.**

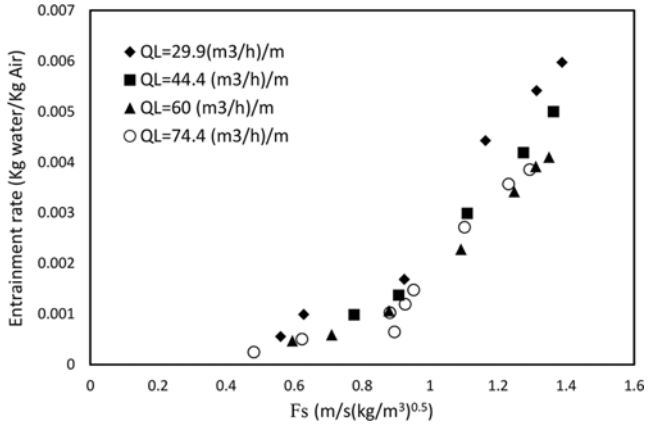


**Fig. 9. Entrainment rate of the valve tray in the various liquid rates: $Q_L$=29.9, 44.4, 60 and 74.4 (m$^3$/h)/m.**

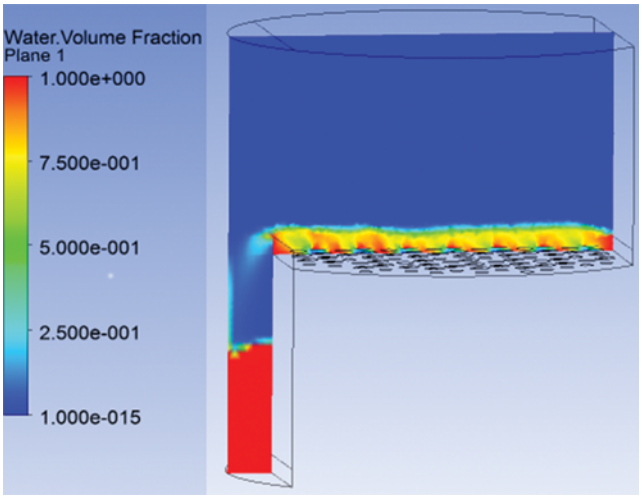


**Fig. 10. Water volume fraction contour in the central plane in $Q_L$= 0.015043283 $m^3/s$ and 0.481754523 $(m/s(kg/m^3)^{0.5})$=$F_S$.**

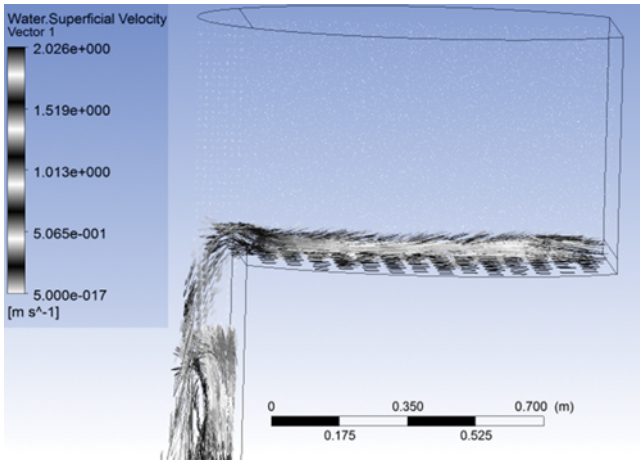


**Fig. 11. Water superficial velocity vector in the central plane in $Q_L$= 0.015043283 $m^3/s$ and $F_S$=0.481754523 $(m/s(kg/m^3)^{0.5})$.**

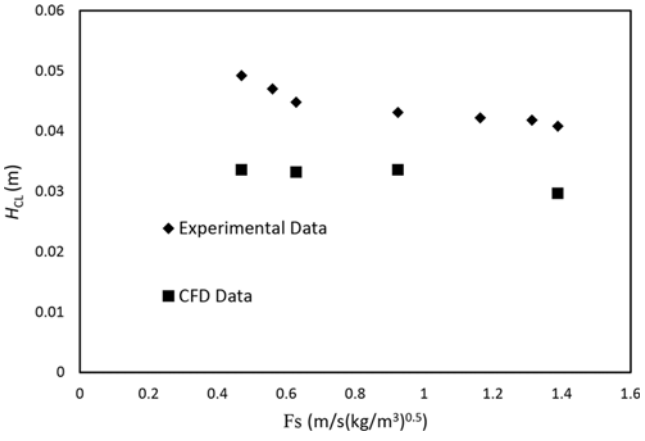


**Fig. 12. Clear liquid height VS. $F_S$ in $Q_L$=0.006061667 $m^3/s$.**

tion of the space in the tray at tray spacing [12].

In Fig. 11, liquid superficial velocity vectors on the tray are shown. As can be seen, entrainment is very low.

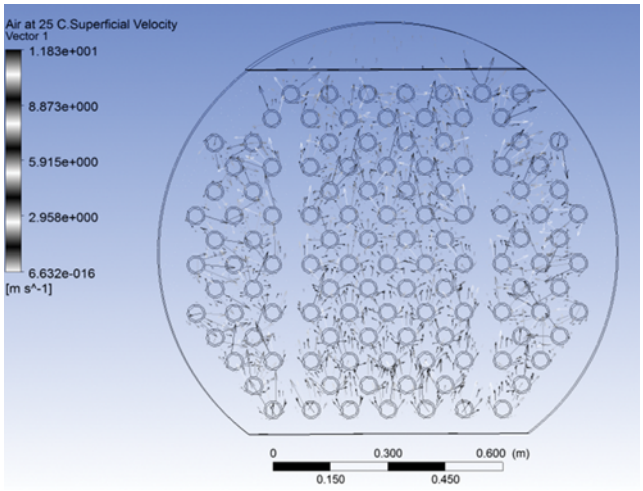


**Fig. 13. Gas velocity vector on the tray deck in $Q_L$=0.012191417 $m^3/s$ and $F_S$=0.907695072 $(m/s(kg/m^3)^{0.5})$.**

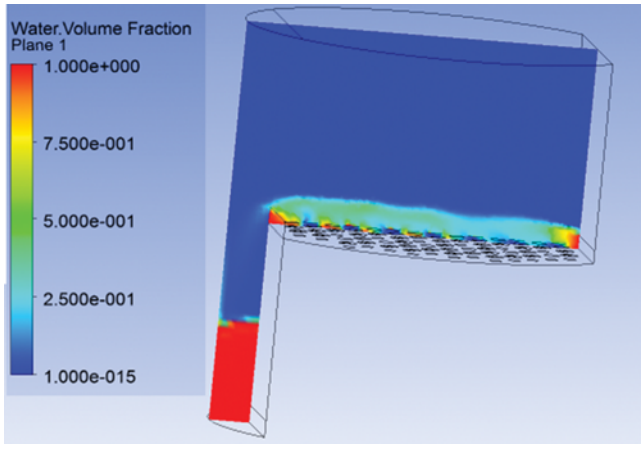


**Fig. 14. Water volume fraction contour at central plane in $Q_L$= 0.00899969 $m^3/s$ and $F_S$=1.362607562 $(m/s(kg/m^3)^{0.5})$.**

The CFD results of the clear liquid height were compared with the experimental data in Fig. 12. The simulation result predicts the experimental data with an average error of about 15%. As seen in Fig. 13, the clear liquid height was decreased by increasing the gas flow rate in both the experiment and simulation.

Fig. 14 shows the velocity vector above the valve's holes. As seen, when the gas was going out of the holes, the gas vertical movement was changed to the horizontal movement, wwhich helps better interfering of liquid and gas phases. This behavior is one the important characteristics of the valve tray which differs from sieve tray.

2-2. Froth Height

Froth height is a layer of spume on trays. In the CFD simulation, in the froth region on the tray, the water volume fraction is more than 10% [7,12]. To obtain this height in the CFD simulation, the average water volume fraction for heights on top of the tray deck was calculated. Where the average volume fraction drops to 10%, this height was selected as froth height. According to these amounts and definition of froth height, this parameter in any oper-

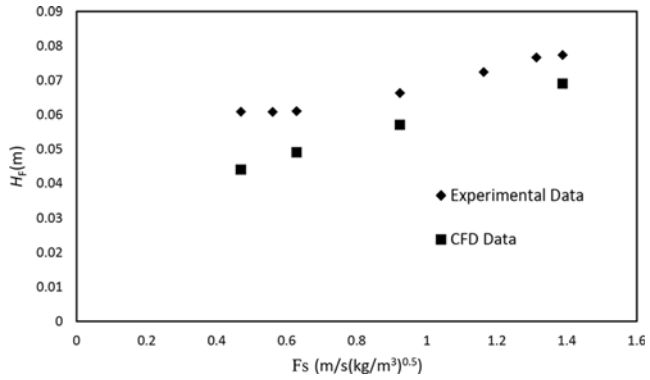


**Fig. 15. Froth height VS. $F_S$ in $Q_L$=0.006061667 $m^3/s$.**

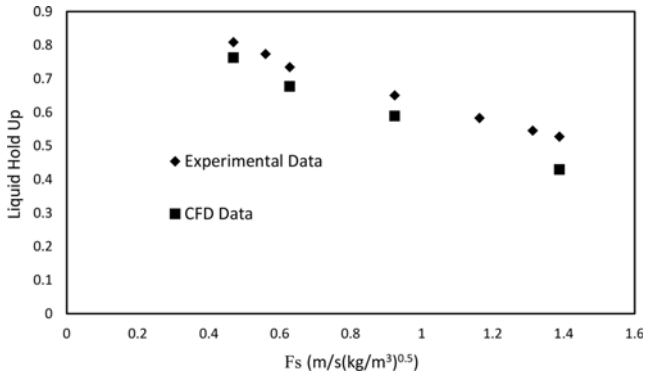


**Fig. 17. Liquid hold up VS. $F_s$ in $Q_L$=0.006061667 $m^3/s$.**

ating conditions was determined.

Fig. 14 is a contour of average liquid holdup in the central plane of the model. As shown, the high gas velocity condition causes to increase the froth height on the tray.

Fig. 15 shows the simulation and experimental data of the froth height. The CFD results can predict the experimental data with 15 percent difference. Both of the CFD and experimental results have the same trends and increased by the increasing the gas flow rate.

Fig. 16 shows the dispersion of the gas phase on the froth region. Dispersion of gas vectors is one of the reasons that this simulation was carried out in three dimensions.

2-3. Average Liquid Holdup

The average liquid holdup is the ratio of the clear liquid height to the froth height. Then, after calculation of the clear liquid and froth height, the average liquid holdup can be achieved. Fig. 17 represents the simulation and experimental data of the average liquid holdup.

Fig. 18 shows the water volume fraction on the tray deck. A uniform liquid distribution on the tray can be observed.

## CONCLUSION

Because experiments for trays have proved to be time-consuming and expensive, only very few attempts have been made so far to determine fluid flow behavior inside industrial trays. Then, to create a better understanding of hydrodynamics of the valve trays, a hydrodynamics tower with two valve trays on an industrial scale was constructed. The results include dry pressure drop, total pressure drop, weeping, entrainment, clear liquid height, froth height and average liquid holdup. As well as according to experimental results the related correlations were obtained.

In the next phase of study, air-water three-dimensional two-phase simulations in an Eulerian framework were carried out. To increase the accuracy of calculations and because of the instability of results in the initial of the tray operations, a transient run was used. The experimental data of the average liquid holdup was used in the drag coefficient for the CFD simulation. This improved the simulation results. From this study, we conclude that with this refined model and interphase momentum transfer relation, we

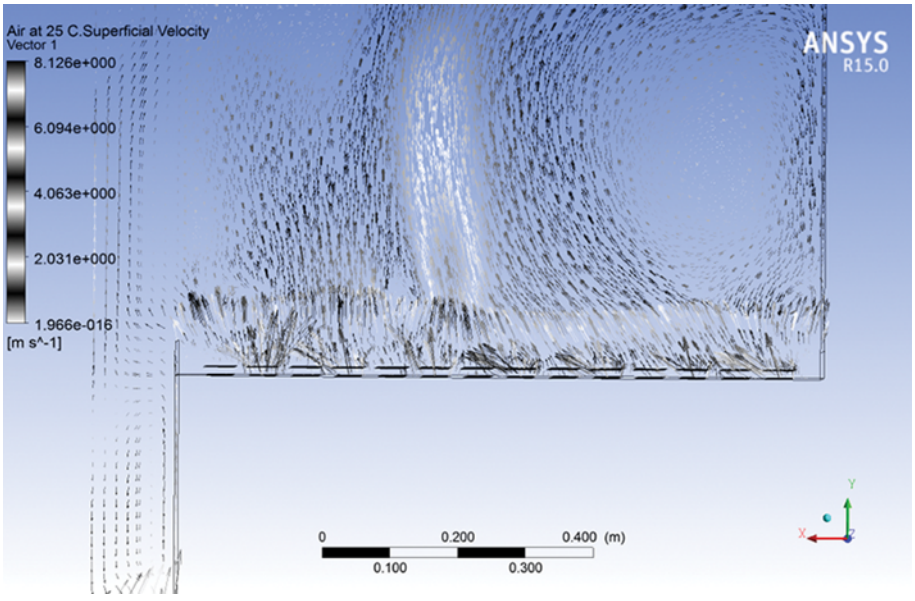


**Fig. 16. Profile of superficial gas velocity in central plane in $Q_L$=0.012191417 $m^3/s$ and $F_S$=0.907695072 $(m/s(kg/m^3)^{0.5})$.**

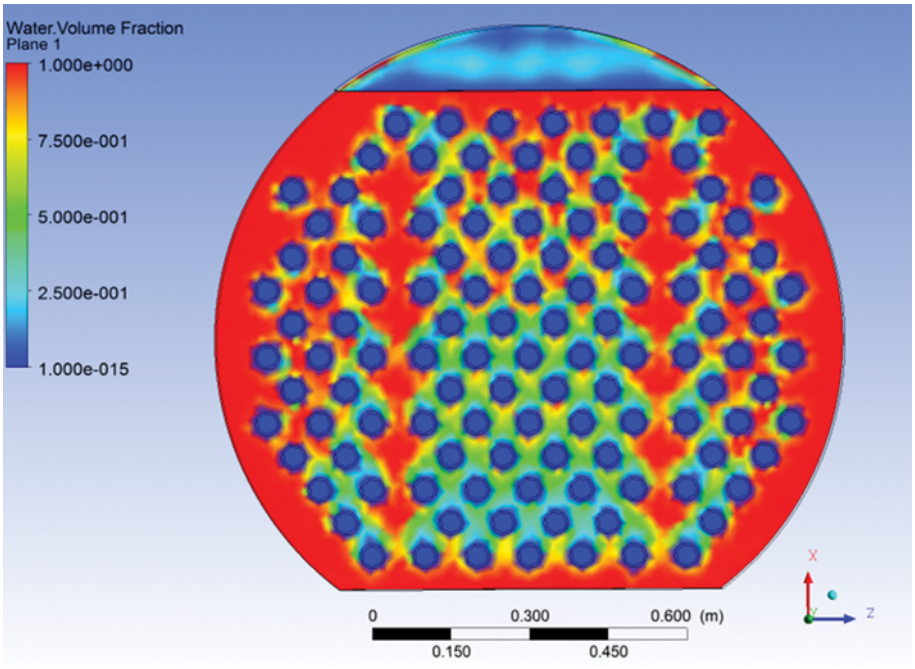


**Fig. 18. Water flow distribution contour on the tray deck.**

were able to get results that closely match the experimental data relative to the previous models which was used from empirical correlations for liquid holdup prediction. Comparison between the CFD and the experimental data shows a 15% difference that indicates a good agreement between them. CFD Modeling overcomes many of the limitations associated with the experiments. So, experimental and CFD simulations must be used together as a prediction and design tool for industrial trays.

## ACKNOWLEDGEMENT

Technical and financial support from Azar Energy Companey is gratefully Acknowledged.

## NOMENCLATURE

$A_{area}$ : active area [$m^2$]
$A_{Hole}$ : area of hole [$m^2$]
$C_D$ : drag coefficient
$d_G$ : diameter of gas bubble [m]
$F_S$ : F-factor=$VS\sqrt{\rho G}$ [$m/s(kg/m^3)^{0.5}$]
g : acceleration of gravity [9.81 $m/s^2$]
$h_{ap}$ : downcomer clearance [m]
$h_{cl}$ : clear liquid height [m]
K : kinetic energy [J]
$L_{weir}$ : weir length [m]
$M_{GL}$ : interphase momentum exchange term [$N/m^3$]
L : length [m]
P : pressure [$kg/m\ s^2$]
$Q_L$ : liquid flow rate across tray [$m^3/s$]
$R^2$ : coefficient of determination
$U_{L,\,in}$ : velocity of liquid inlet [m/s]
$U_{L,\,max}$ : maximum velocity of liquid [m/s]
V, U : velocity [m/s]
$V_{Airin}$ : velocity of gas inlet [m/s]
$V_S$ : superficial gas velocity [m/s]
$V_{slip}$ : slip velocity between gas and liquid [m/s]
x : coordinate [m]
y : coordinate [m]
Z : coordinate [m]

### Greek Letters

α : volume fraction of phase
μ : viscosity of phase [pa·s]
ρ : density of phase [$kg/m^3$]
ε : gradient of kinetic energy
$\mu_{eff}$ : effective viscosity of phase

### Subscripts

cl : clear liquid
G : referring to gas phase
L : referring to liquid phase
max : maximum
In : inlet

## REFERENCES

1. R. D. Scheffe and R. H. Weiland, *Ind. Eng. Chem. Res.*, **26**, 228 (1987).
2. H. Mustafa and E. Békássy-Molnár, *Chem. Eng. Res. Des.*, **75**(6), 620 (1997).
3. E. F. Wijn, *Chem. Eng. J.*, **70**, 143 (1998).
4. R. Brahem, A. Royon-Lebeaud, D. Legendre, M. Moreaud and L. Duval, *Chem. Eng. Sci.*, **100**, 23 (2013).

5. R. Krishna, J. M. van Baten, J. Ellenberger, A. P. Higler and R. Taylor, *Chem. Eng. Res. Des., Trans. I. Chem. E*, **77**, 639 (1999).
6. J. M. van Baten and R. Krishna, *Chem. Eng. J.*, **77**, 143 (2000).
7. G. Gesit, K. Nandakumar and K. T. Chuang, *AIChE J.*, **49**(4), 910 (2003).
8. S. Roshdi, N. Kasiri, S. H. Hashemabad and J. Ivakpour, *Korean J. Chem. Eng.*, **30**, 563 (2013).
9. A. Zarei, S. H. Hosseini and R. Rahimi, *J. Taiwan Institute Chem. Engineers*, **44**, 27 (2013).
10. F. J. Zuiderweg, *Chem. Eng. Sci.*, **37**, 1441 (1982).
11. X. G. Li, D. X. Liu, S. M. Xu and H. Li, *Chem. Engin. Proc.*, **48**, 145 (2009).
12. T. Zarei, R. Rahimi and M. Zivdar, *Korean J. Chem. Eng.*, **26**(5), 1213 (2009).
13. B. Solari and R. L. Bell, *AIChE J.*, **32**, 640 (1986).
14. A. Alizadehdakhel, M. Rahimi and A. Abdulaziz Alsairafi, *Comput. Chem. Eng.*, **34**, 1 (2010).
15. S. Jiang, H. Gao, J. Sun, Y. Wang and L. Zhang, *Chem. Eng. Process: Process Intensification*, **52**, 74 (2012).
16. M. Yufeng, J. Lijun, Z. Jiexu, C. Kui, W. Bin, W. Yanyang and Z. Jiawen, *Chinese J. Chem. Eng.*, **23**(10), 1603 (2015).
17. M. J. Lockett, *Distillation Tray Fundamentals*, Cambridge University Press, New York (1986).
18. H. Z. Kister, *Distillation design*, Boston (1992).
19. V. V. Ranade, *Computational flow modeling for chemical reactor engineering*, Academic Press (2001).
20. D. Lakehal, *Int. J. Multiphase Flow*, **28**, 823 (2002).
21. D. L. Bennett, R. Agrawal and P. J. Cook, *AIChE J.*, **29**, 434 (1983).
22. Y. Jianping and Y. Shurong, *Adv. Mechanical Eng.*, **7**(11), 1 (2015).
23. R. Rahimi, A. Zarei, T. Zarei, H. N. Firoozsalari and M. Zivdar, In Distillation Absorption Conference, 407 (2010).
24. E. Jia-qiang, L. Yu-qiang and G. Jin-ke, *J. Cent. South Univ. Technol.*, **18**, 1733 (2011).